IEEE Photonics Journal
An IEEE Photonics Society Publication

Open Access

Crosstalk Analysis of SiC Ultraviolet Single Photon Avalanche Photodiode Arrays

Volume 11, Number 6, December 2019

Heng Zhang
Linlin Su
Dong Zhou
Weizong Xu
Fangfang Ren
Dunjun Chen
Rong Zhang
Youdou Zheng
Hai Lu

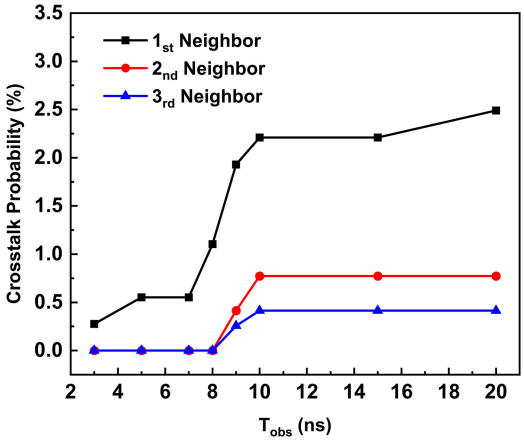

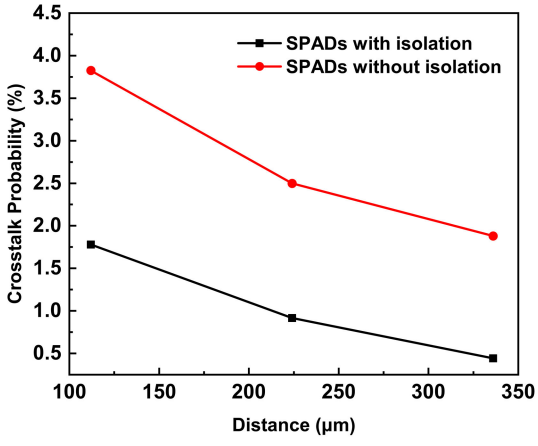

DOI: 10.1109/JPHOT.2019.2954119

Crosstalk Analysis of SiC Ultraviolet Single Photon Avalanche Photodiode Arrays

Heng Zhang, Linlin Su, Dong Zhou, Weizong Xu, Fangfang Ren, Dunjun Chen, Rong Zhang, Youdou Zheng, and Hai Lu

School of Electronic Science and Engineering Collaborative Innovation Center of Advanced Microstructures, Nanjing University, Nanjing 210093, China

DOI:10.1109/JPHOT.2019.2954119

Manuscript received August 17, 2019; accepted November 13, 2019. Date of publication November 18, 2019; date of current version December 17, 2019. This work was supported in part by the National Key R&D Program of China under Grant 2016YFB0400902 and in part by the National Natural Science Foundation of China under Grant 61921005. Corresponding author: Hai Lu (e-mail: hailu@nju.edu.cn).

Abstract: Optical crosstalk is one of major problems limiting the performance of focal plane arrays based on single photon avalanche diodes (SPADs). In this work, for the first time the crosstalk characteristics of a 4H-SiC SPAD linear array are studied, which is based on a real-time dual channel data acquisition method. It is found that SiC SPAD array exhibits similar crosstalk probability compared with those of InGaAs-based SPAD arrays, which can be effectively reduced by trench isolation between adjacent pixels or by lowering overbias. The average time required for forming a crosstalk event is determined between 7 and 10 ns. As a result, active time-gated operation scheme can be applied for reducing crosstalk.

Index Terms: SiC, SPAD array, ultraviolet, crosstalk.

1. Introduction

Nowadays, ultraviolet (UV) focal plane array (FPA) based on SiC single photon counting avalanche photodiodes (SPADs) has attracted much attention due to its potential to replace traditional microchannel plate (MCP) based image intensifiers, which are key components for many cutting-edge applications, such as missile plume detection and tracking, solar physics as well as chemical/biological agent detection [1], [2], [3]. In addition, since atmospheric molecules could strongly scatter UV light, laser radars based on UV detector array have important applications for atmospheric condition and wind speed monitoring [4], [5]. Compared with vacuum devices, SPAD-based FPAs have many potential advantages, such as high quantum efficiency, low weight, lower operation voltage and long lifetime [6].

To improve imaging resolution and quantum efficiency, there is continuous effort to enhance fill factor of each pixel and reduce pixel spacing in FPA design. Nevertheless, an increasing limitation of densely packed SPAD arrays is undesirable optical crosstalk, which would degrade signal-to-noise ratio of imaging systems [7]. When a dark count or a real photon count occurs, a large number of electrons and holes would generate by avalanche multiplication and some of them might recombine to produce secondary photons, which could couple to nearby SPADs in the array and introduce spurious counts. In the case of an InGaAs/InP SPAD array with a pixel spacing of 100 μm, the crosstalk probability between two neighboring SPADs has been determined $\sim$2%, and the total

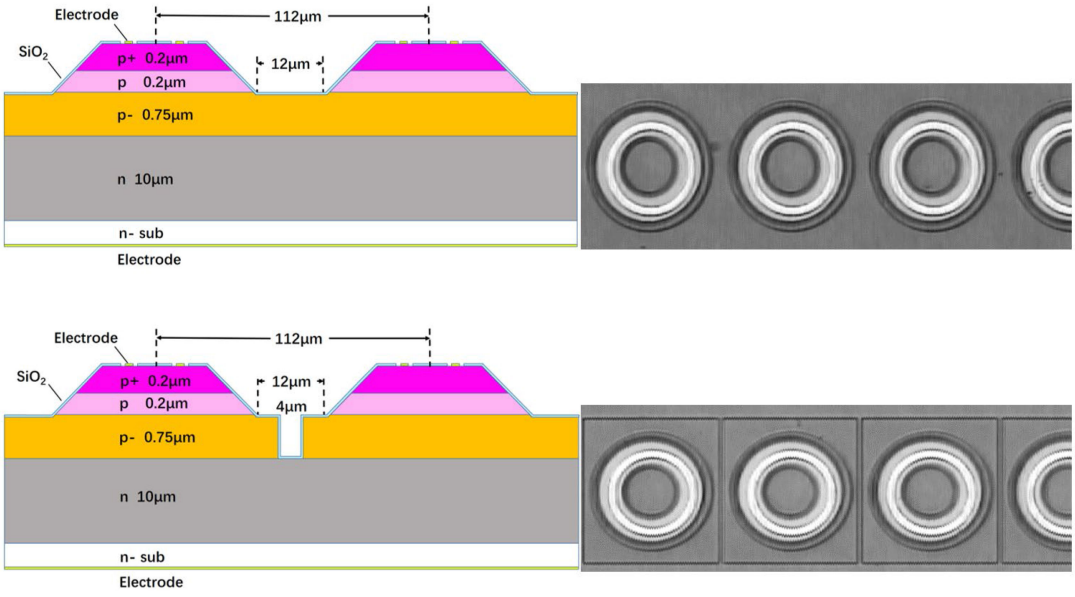

Fig. 1. Cross-sectional schematic and top view of two types of SiC SPAD linear array, showing the distances between adjacent devices. SPADs are fabricated on the same substrate.

integrated crosstalk probability is found under 15% [8]. Many experiments have shown that optical crosstalk is a serious counting error factor in highly integrated SPAD FPAs [9], [10], [11].

In this work, linear arrays based on SiC UV SPADs are designed and fabricated with and without trench isolation. Crosstalk characteristics of the SPAD linear array are studied for the first time. It is determined that SiC SPAD array exhibits similar crosstalk probability compared with those of InGaAs-based SPAD arrays at comparable pixel spacing. The relationship between crosstalk probability and overbias applied on the SiC SPADs is analyzed. The work may provide a useful guidance for design of FPAs based on SiC UV SPADs.

2. Experimental Details

The cross-sectional schematic of the SiC SPAD linear arrays studied in this work is shown in Fig. 1. The epi-structure is grown on 4-inch n-type 4H-SiC substrate, which from bottom to top consists of a 10 μm n+ buffer layer, a 0.75 μm p- multiplication layer, a 0.2 μm p transition layer and a 0.2 μm p+ contact layer. The fabrication procedure begins with mesa etching, which is conducted in an inductively coupled plasma etching system with CF_4/O_2 as the etching gas. Using a photoresist reflow technique, the device mesa inherits the shape of the photoresist. A positive beveled mesa with a low slope angle of $\sim$5° is achieved, which is effective to suppress edge breakdown [12], [13]. The SPAD pixel has a circular shape with a typical mesa diameter of $\sim$100 μm. Two types of 1$\times$128 SiC SPAD linear arrays are fabricated. One has a 4 μm-wide trench isolation down to the n+ buffer layer between adjacent pixels while the other has no special trench isolation. The trench etching is done by using a hard mask. Then the device surface is passivated by SiO_2 layer deposited by plasma-enhanced chemical vapor deposition. After opening the contact windows by wet etching, p top metal contact and n bottom contact both using Ni/Ti/Al/Au metal stack are deposited by e-beam evaporation, which are finally annealed by rapid thermal annealing in N_2 ambient.

Fig. 2(a) shows typical room temperature current-voltage curves of the SiC SPADs. The breakdown voltage (V_b) is $\sim$227 V, which is signaled by a sharp increase of reverse current. The V_b difference of SiC SPADs with and without trench isolation is quite close and less than 0.5 V, which means that the trench outside the mesa area would not disturb electrical field distribution within the SPAD. The single photon detection characteristics of the SPADs are measured by using a

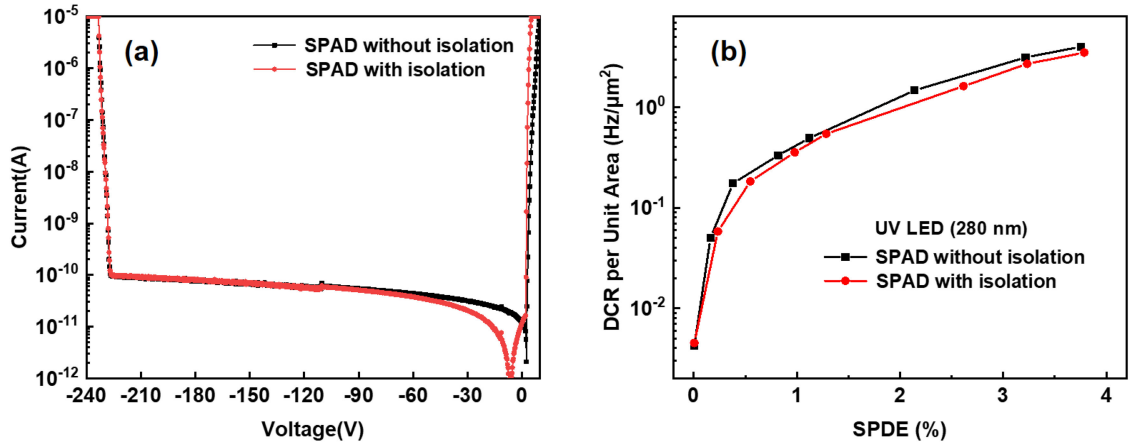

Fig. 2. (a) Current-voltage characteristics of two types of SPADs. (b) DCR vs. SPDE characteristics of the SPADs.

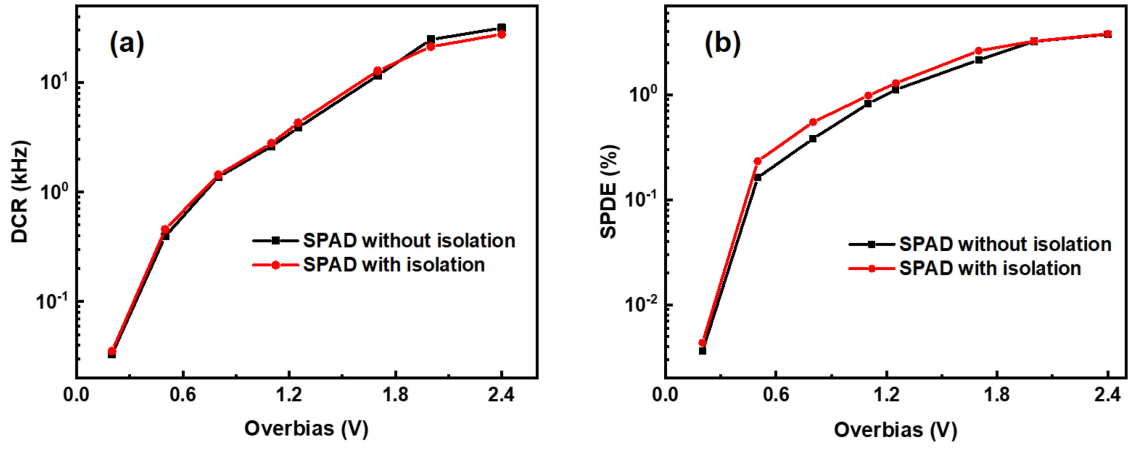

Fig. 3. (a) DCR vs. overbias and (b) SPDE vs. overbias characteristics of the SPADs.

passive quenching circuit, in which the load resistor is set as zero and the SPAD is quenched by its self-resistance [14], [15]. Self-quenching mode could reduce recovery time caused by RC effect, which is beneficial for time correlated crosstalk analysis [16]. Single photon detection efficiency (SPDE) vs dark count rate (DCR) is evaluated at room temperature, which uses a 280 nm deep UV light emitting diode as the light source (see Fig. 2(b)). Again, the SiC SPADs with and without trench isolation show similar performance. Specifically, when the SPDE is fixed ~3%, the corresponding DCR is determined ~3 Hz/μm^2. In addition, Fig. 3 shows that the two types of SPADs have no obvious difference in terms of DCR vs overbias and SPDE vs overbias characteristics.

Crosstalk characteristics are studied by pseudo-crosstalk measurement, in which the count-rate of a SPAD is evaluated while another SPAD is operating as emitter. As shown in Fig. 4(a), both devices are being biased above breakdown at same overbias with common cathode and respective sampling resistors. Real-time output voltage pulses from the two SPADs are recorded by a dual-channel oscilloscope. The experiment is conducted under dark. That is, only noise pulses originated by thermal current and tunneling current are counted. Coincidence analysis is applied to study the temporal correlation between the output signals generated in neighboring pixels, which allows to obtain crosstalk probability directly [7]. As illustrated by Fig. 4(b), only pulse pairs with sufficiently small time interval are regarded as a crosstalk event. In order to achieve an acceptable

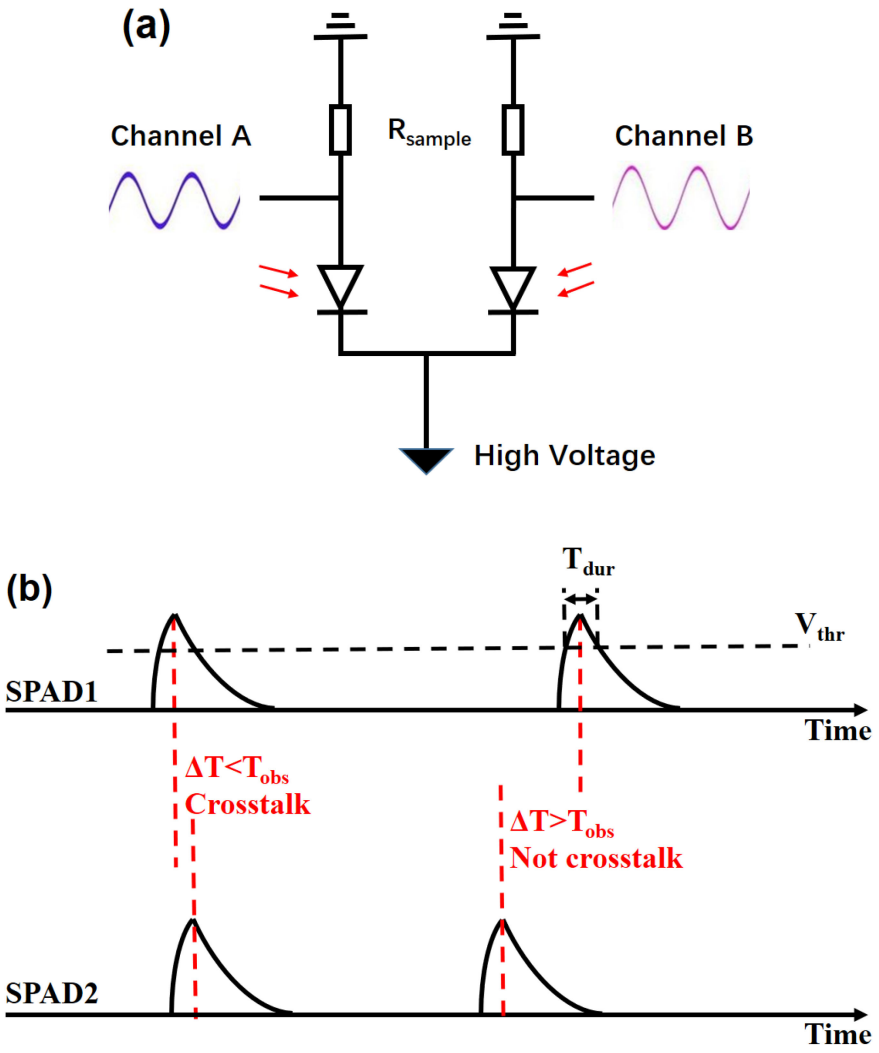

Fig. 4. (a) The experiment method: A positive high voltage is added at the common cathode, and sampling resistors for signal extraction are connected at the anode. Oscilloscope's dual channels are used to record voltage values; (b) The diagram of crosstalk analysis, showing the three parameters, V_{thr}, T_{dur}, T_{obs}.

signal-to-noise ratio, the crosstalk measurement requires long acquisition time, which consists of a large number of cycles (over 10^7) made of two adjacent output pulses.

In the data analysis algorithm, there are three key parameters, i.e., count threshold voltage V_{thr}, pulse duration time T_{dur} and crosstalk observation time T_{obs}. Here, V_{thr} is mainly limited by noise floor of the test circuit, which is set as 8 mV to avoid false counts. T_{dur} is the obtained average pulse width for a single count, which is set as 300 ns. During this time period, multiple voltages exceeding the threshold are recorded as a counting pulse. T_{obs} is the judgement standard for whether or not crosstalk occurs, which represents crosstalk formation time and is experimentally determined. The interval between unrelated counts should be much larger than 10ns when the DCR of SPADs is around 20 kHz. A crosstalk is recognized only if two adjacent pulses from the two SPADs have a time interval less than T_{obs} (see Fig. 4(b)). In the context of a large number of statistics, the crosstalk probability is obtained by dividing the number of crosstalk events by the total count. Fig. 5 shows the real time output waveforms of the SPADs and the enlarged portion of waveforms illustrating a crosstalk. It is clear that the RC oscillations following a real count pulse could somewhat degrade

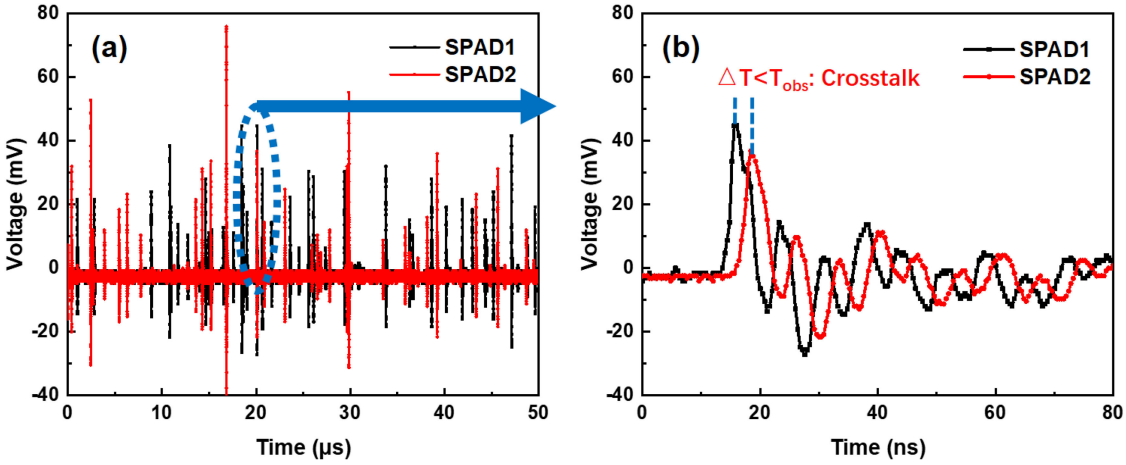

Fig. 5. (a) Selected real time output waveforms of the "emitter" and the "receiver" SPADs; (b) the enlarged portion of waveforms illustrating a crosstalk.

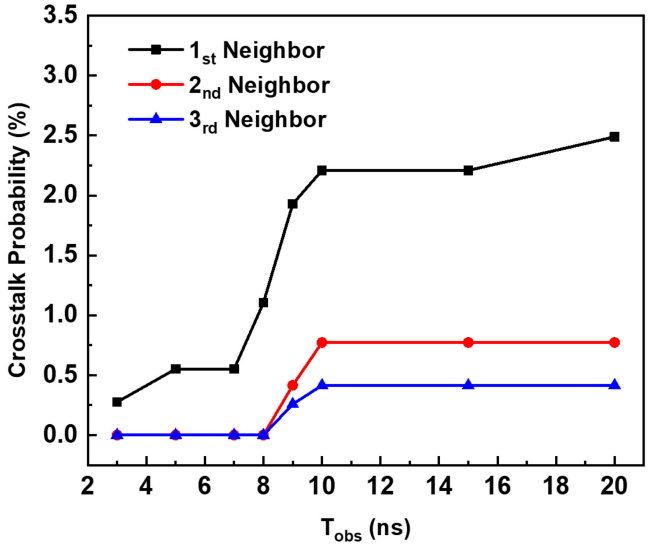

Fig. 6. Crosstalk probability as a function of observation time T_{obs} when overbias on the isolated SPAD pair is set as 2.0 V.

signal quality. This negative effect is reduced by setting a high T_{dur} value of 300 ns, which has also been used for DCR and SPDE characterization.

3. Results and Discussion

Fig. 6 shows the crosstalk probability calculated as a function of chosen T_{obs} for the 1st, 2nd, and 3rd neighbor pixels. The purpose of this analysis is to find a suitable T_{obs} for accurate characterization of crosstalk probability in later study. During the measurements, the SPAD pairs are biased at 229.5 V with a mean room temperature DCR of around 15 kHz. The difference of DCR between the two devices is less than 3 kHz. It is found that as observation time increases, the crosstalk probability rises steeply after 7 ns and tends to be stable after 10 ns. Meanwhile, the overall crosstalk probability is higher for close neighbor pixels. Presumably, the formation time of a crosstalk includes carrier recombination time, photon propagation time and avalanche buildup time. The propagation time of photons among pixels should be very short and then T_{obs} is mainly

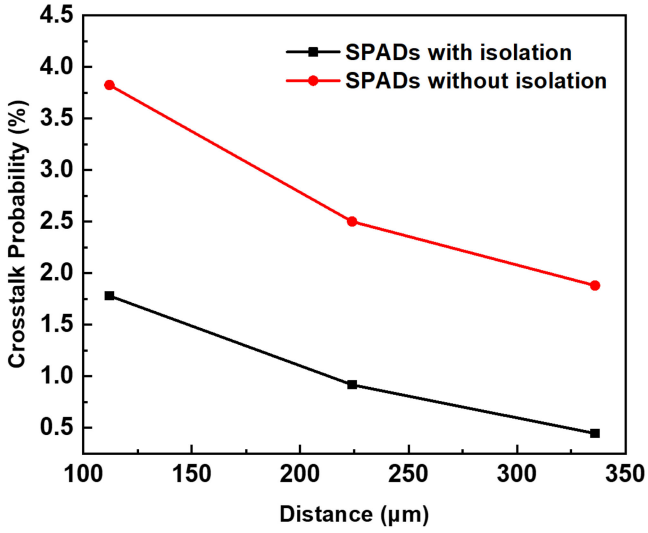

Fig. 7. The relationship between optical crosstalk probability and device spacing in the two types of SPAD arrays.

made up of the other two factors. The above result means that the formation time of a crosstalk in the SiC SPAD array is mostly distributed between 7–10 ns, which is very close to the T_{obs} value of 10 ns found in Si SPAD array systems [7].

Considering that long observation time would introduce unnecessary interference between different crosstalk events, T_{obs} is set as 10 ns in the following analysis. Fig. 7 shows the crosstalk probability of the SiC SPAD arrays as a function of device center-to-center distance. Here two facts can be clearly observed. Firstly, SiC SPAD array with trench isolation has at least one fold lower crosstalk probability than that of SPAD array without trench isolation. This can be easily understood as the trench would not only effectively block carrier diffusion path between adjacent pixels, but also would suppress photon propagation probability through surface/interface reflections. As illustrated in Fig. 1(b), the trench would introduce a SiC/SiO_2/air/SiO_2/SiC multiple interface structure. Secondly, the crosstalk probability would quickly drop as pixel inter-spacing increases. Specifically, as the device center-to-center distance increases from 120 to 360 μm, the crosstalk probability for the SPAD array with trench would reduce from 1.75 to 0.5%. These numbers are close to the crosstalk probability values of InGaAs/InP SPAD arrays and Si SPAD arrays reported in literature, which validates the analysis method applied in this work [8].

Besides geometrical factors, crosstalk probability also strongly depends on the degree of avalanche multiplication. As shown in Fig. 8, the crosstalk probability of 1st neighbor pixel pairs would rise quickly at higher device overbias. Considering the detailed process of a crosstalk, the crosstalk probability $P_{crosstalk}$ can be roughly calculated by the following equation:

$$P_{crosstalk} = P_{generation} \times P_{pass} \times P_{absorb} \times P_{avalanche}$$

in which $P_{generation}$ is the recombination probability of multiplied photo-carriers in the transmitting SPAD, P_{pass} is the probability that a photon could propagate to the receiving SPAD, P_{absorb} is the absorption probability of photons by the receiving SPAD, and $P_{avalanche}$ is the probability that the newly excited photo-carriers could trigger an avalanche event. It is expected that $P_{generation}$ is mainly determined by the band structure of the semiconductor material, which is low for 4H-SiC due to its indirect band structure. In addition, by introducing special structures like multi-quantum-wells and artificial defects, the photon generation rate can be enhanced, which is nevertheless not the case for the current SiC SPAD. P_{pass} is mainly determined by the structure of the SPAD array. As has been revealed, trend isolation can effectively reduce P_{pass}. There is also report that the patterned electrode on the illumination side of the SPAD array could partially suppress internal

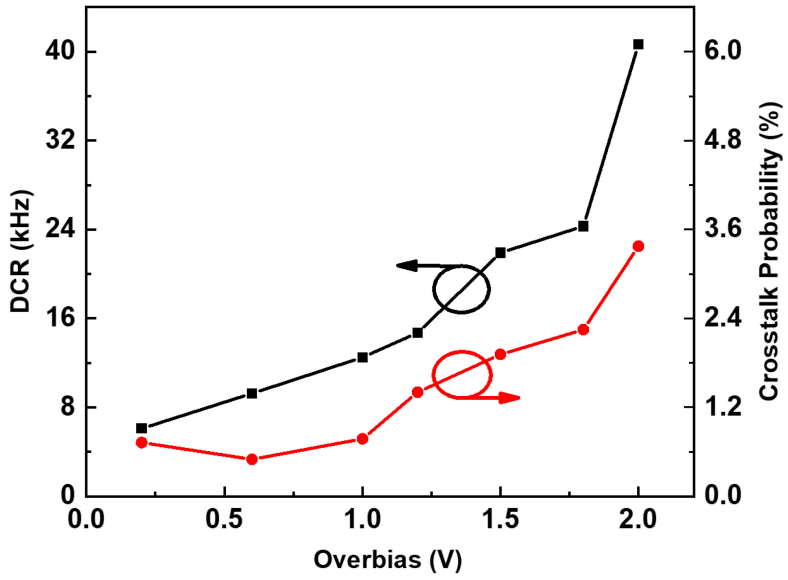

Fig. 8. DCR vs. overbias and crosstalk probability (1st neighbor) vs. overbias characteristics of the SiC SPAD array without trench isolation.

reflection and thus reduce P_{pass} [9]. In addition, optical absorption along the propagation path of photons from the "emitter" pixel to the "receiver" pixel should also reduce P_{pass}. P_{absorb} is mainly influenced by the optical absorption coefficient of SiC, which also correlates with the absorption layer thickness of the SPAD. Finally, it is clear that enhancing overbias would increase electric field strength within the SPAD multiplication layer, which would lead to a rapid increase of $P_{avalanche}$ while the other three factors are less affected. Meanwhile, it is found that DCR of the SPAD grows with a similar trend to that of $P_{crosstalk}$ as a function of overbias. This agrees with the above analysis that variation of $P_{avalanche}$ is the dominate factor. Thus, in future application of SiC SPAD arrays, besides the trade-off between DCR and SPDE, choosing a suitable overbias is also important for limiting the magnitude of crosstalk probability.

4. Conclusion

In this work, the crosstalk probability of SiC-based SPAD arrays is characterized for the first time, which is found on the similar level compared with that of traditional InGaAs or Si based SPAD arrays. The crosstalk probability can be considerably reduced by adding trench isolation between SPAD pixels, or by decreasing excess bias. The formation time of a crosstalk in the SiC SPAD array is found consistently between 7 and 10 ns. This observation may give a hint to solve the crosstalk problem, which could be reduced by active time-gated operation scheme in imaging process. This study could provide a useful guidance for future applications of FPAs based on SiC SPAD arrays.

References

[1] M. Razeghi, "Short-wavelength solar-blind detectors-status, prospects, and markets," *Proc. IEEE*, vol. 90, no. 6, pp. 1006–1014, Jun. 2002.
[2] G. A. Shaw *et al.*, "Deep UV photon-counting detectors and applications," *Proc. SPIE*, vol. 7320, 2009, Art. no. 73200J.
[3] M. A. Albota *et al.*, "Three-dimensional imaging laser radar with a photon-counting avalanche photodiode array and microchip laser," *Appl. Opt.*, vol. 41, no. 36, pp. 7671–7678, 2002.
[4] O. Uchino, M. Maeda, and M. Hirono, "Applications of excimer lasers to laser-radar observations of the upper atmosphere," *IEEE J. Quantum Electron.*, vol. QE-15, no. 10, pp. 1094–1107, Oct. 1979.
[5] E. Nava and E. Stucchi, "Development of lasers for spaceborne Doppler wind lidar applications," *Opt. Lasers Eng.*, vol. 39, no. 2, pp. 255–263, 2003.

[6] A. Katsushi, "New trends in vacuum-based photon detectors," *Nucl. Instrum. Methods Phys. Res. Sect. A, Accel., Spectrometers, Detect. Associated Equip.*, vol. 442, no. 1/3, pp. 80–90, 2000.
[7] A. Vilà, E. Vilella, O. Alonso, and A. Dieguez, "Crosstalk-free single photon avalanche photodiodes located in a shared well," *IEEE Electron Device Lett.*, vol. 35, no. 1, pp. 99–101, Jan. 2014.
[8] M. A. Itzler *et al.*, "Geiger-mode avalanche photodiode focal plane arrays for three-dimensional imaging LADAR," *Proc. SPIE*, vol. 7808, 2010, Art. no 78080C.
[9] R. D. Younger *et al.*, "Crosstalk analysis of integrated Geiger-mode avalanche photodiode focal plane arrays," *Proc. SPIE*, vol. 7320, 2009, Art. no. 73200Q.
[10] B. Piccione, X. Jiang, and M. A. Itzler, "Spatial modeling of optical crosstalk in InGaAsP Geiger-mode APD focal plane arrays," *Opt. Exp.*, vol. 24, no. 10, pp. 10635–10648, 2016.
[11] B. F. Aull, D. R. Schuette, D. J. Young, D. M. Craig, B. J. Felton, and K. Warner, "A study of crosstalk in a 256∗256 photon counting imager based on silicon Geiger-mode Avalanche photodiodes," *IEEE Sensors J.*, vol. 15, no. 4, pp. 2123–2132, Apr. 2015.
[12] D. Zhou *et al.*, "High-temperature single photon detection performance of 4H-SiC avalanche photodiodes," *IEEE Photon. Technol. Lett.*, vol. 26, no. 11, pp. 1136–1138, Jun. 2014.
[13] S. Yang *et al.*, "4H-SiC ultraviolet avalanche photodiodes with small gain slope and enhanced fill factor," *IEEE Photon. J.*, vol. 9, no. 2, Mar. 2017, Art. no. 6801508.
[14] L. Fei *et al.*, "Passive quenching electronics for Geiger mode 4H-SiC avalanche photodiodes," *Chin. Phys. Lett.*, vol. 32, no. 12, 2015, Art. no. 128501.
[15] J. Cheng, S. You, S. Rahman, and Y.-H. Lo, "Self-quenching InGaAs/InP single photon avalanche detector utilizing zinc diffusion rings," *Opt. Exp.*, vol. 19, no. 16, pp. 15149–15154, 2011.
[16] M. A. Itzler, X. Jiang, B. M. Onat, and K. Slomkowski, "Progress in self-quenching InP-based single photon detectors," *Proc. SPIE*, vol. 7608, 2010, Art. no. 760829.